Journal of Computational and Theoretical Nanoscience
Vol. 8, 1278–1287, 2011

Chirality Transfer from Molecular to Morphological Scales in Quasi-One-Dimensional Nanomaterials: A Continuum Model

Jian-Shan Wang[1,*], Xi-Qiao Feng[2,*], Jun Xu[3], Qing-Hua Qin[4], and Shou-Wen Yu[2]

[1] *Department of Mechanics, Tianjin University, Tianjin 300072, China*
[2] *Department of Engineering Mechanics, AML, Tsinghua University, Beijing 100084, China*
[3] *Institute of Polymer Science and Engineering, Department of Chemical Engineering, School of Materials Science and Technology, Tsinghua University, Beijing 100084, China*
[4] *School of Engineering, Australian National University, Canberra, ACT 0200, Australia*

Structural hierarchy of chirality is observable in a diversity of biological and synthetic materials and related to some unusual physical properties. The transfer of chirality among different length scales is a crucial issue of both theoretical and technological interest. In this paper, a continuum model is developed to phenomenologically rationalize the chirality transfer from the constituent molecules to geometric morphology of quasi-one-dimensional nanomaterials. We demonstrate that the competition or cooperative interactions between lower-level chirality and surface effects may lead to the formation of various asymmetric geometric shapes. The twisting handedness and pitch length of chiral morphologies of quasi-one-dimensional materials is derived in terms of materials chirality and anisotropic surface stresses. The inversion of morphological chirality observed in experiments is also explained in this paper. The results of the study is useful not only for understanding various interesting phenomena associated with chirality but also for optimal design and fabrication of novel materials and devices with enhanced properties and functions.

Keywords: Quasi-One-Dimensional Nanomaterials, Chiral Materials, Chirality, Surface Effect, Size Effect.

1. INTRODUCTION

The word *chirality*, coined by Lord Kelvin, refers to the configurational properties of an object that is not superimposable on its mirror image.[1,2] The absence of mirror symmetry of constituent molecules, microstructures and even morphologies of biological and synthetic materials (e.g., quasi-one-dimensional nanomaterials) has a remarkable effect on their physical properties and functions.[3–6] For example, the morphological chirality in twisted nanobelts and nanohelices (they can be made of either metals, semiconductors or polymers) makes them have some superior elastic properties and unusual electrical or optical properties.[6,7] In recent years, manipulating specific morphological chirality has been actively pursued as an effective means to tailor the physical properties and even specified functions of micro/nano-sized materials and devices which hold many technologically important applications in, for instance, optoelectronic devices, chirality recognition and separation, chiral imprinting, and microelectromechanical systems.[7] Therefore, understanding the physical mechanisms underlying the formation of chiral morphologies at micro and nano scales is of great significance from both scientific and practical points of view.

There exist many possible physical mechanisms that may cause the formation of morphological chirality of materials at micro and nano scales. For metals, semiconductor and polymer materials, the dominant factors driving the formation of chiral morphologies (e.g., twisting nanobelts and nanohelices) are often different. Roughly speaking, the existence of anisotropic interactions or external forces during the growth or fabrication process of materials manifests some chiral morphologies.[8] For example, the formation of helices of such biopolymers as DNA and viral capsids has been understood from the angles of entropy and regular assembly of identical objects.[9,10] The helical growth of amorphous boron carbide nanospring has been attributed to its anisotropic contact with the adopted catalyst.[11] Some other physical mechanisms underlying

*Authors to whom correspondence should be addressed.

 1546-1955/2011/8/1278/010 doi:10.1166/jctn.2011.1811

the appearance of morphological chirality in materials include the microstructural features or the asymmetric evolution or instability of defects (e.g., dislocations and interfaces) at micro and nano scales. For the polymer lamellar twisting manifested by spherulite bands, unbalanced surface stresses has been experimentally confirmed as an important mechanical origin.[12] Recently, we theoretically addressed the effect of anisotropic surface stresses on the formation of twisting nanowire and helical nanobelts.[13] We also tuned the lamellar twisting chirality of microbial poly(R-3-hydroxybutyrate) copolymers via copolymerization or blending, providing a more direct evidence for the significance of anisotropic surface stresses.[14]

For a wide range of synthetic materials, biological and self-assembled systems at micro and nanoscale, the formation of such chiral morphologies as twisting lamellae and nanohelices origins from a process of transfer of chirality. Chirality transfer in such materials as self-assembled chiral fibrillar networks and aggregates,[15, 16] nanostructured chiral molecular gel,[17] and helical ribbons of chiral lipid bilayer[18] has been widely addressed in the literatures. For those systems with hierarchical structures, chiral morphologies are often macroscopic reflections of chemical chirality (e.g., molecular and conformational chirality) and microstructural chirality (e.g., helical monodomains or crystals, Eshelby twist[7]) at lower levels. During the growth of chiral polymer lamellae, for example, chirality are transferred from molecular level to helical chain structures, then to chain folding organization on the lamellar surface, and eventually to the macroscopic level (twisting lamellae and even clustering of crystals and polymer spherulites),[19] as shown in Figure 1.

Morphological chirality depends usually on the chirality of its basic constituent elements (e.g., chiral molecules aggregates, helical chains and microstructures) at smaller length scales. The chirality at a lower structural level can be mapped into the macroscopic morphologies of materials. Chirality transfer can also be used to design engineering chiral materials e.g., chiral fibres, twisting nanobelts, and nanohelices. For instance, the helical chain units are used to fabricate the chiral materials with desired physical properties in the area of solid-state chemistry.[21] Helfrich[22] theoretically proved that if the isotropic cross-section of a fiber consists of chiral molecules, it will prefer a helical shape. Such a transfer from the chirality at a lower length level to a higher is also referred to as the "chirality effect" for the chiral polymer growth, chiral molecular packing, and chiral fibre self-assembly.[12, 16] However, the interactions between chiral elements and other factors such as intermolecular forces (e.g., hydrogen bonding, van der Waals and electrostatic forces),[23] the rigidity and length of chains and residual stresses also influence the chirality transfer among different length levels in a complicated manner. Due to these reasons, the chirality information at a lower level may be lost at a higher level, and the macroscopic morphological chirality of a material is closely but not univoqually correlated with that of its constituent elements.[12] In the case of chiral polymer, for example, it has been shown that besides configurational chirality of molecules and helical chain, unbalanced anisotropic surface stresses also play an important role in the twisting growth of lamellas.[12] Both right- and left-handed chiral morphologies can be induced by molecules with identical chirality.[24, 25]

Another interesting and yet unresolved issue is the quantitative characterization of various chiralities at different length scales. The quantitative description of chirality can only be characterized either by physical properties or geometric parameters.[26] In addition, for quasi-one-dimensional nanomaterials or self-assembled systems with a hierarchy of chirality, chirality transfer from molecular level to macroscopic morphologies involves complicated multi-scale interactions of different chirality at various structural levels. Furthermore, the chirality transfer in quasi-one-dimensional nanomaterials also exhibits distinct size dependence due to the large surface-to-volume

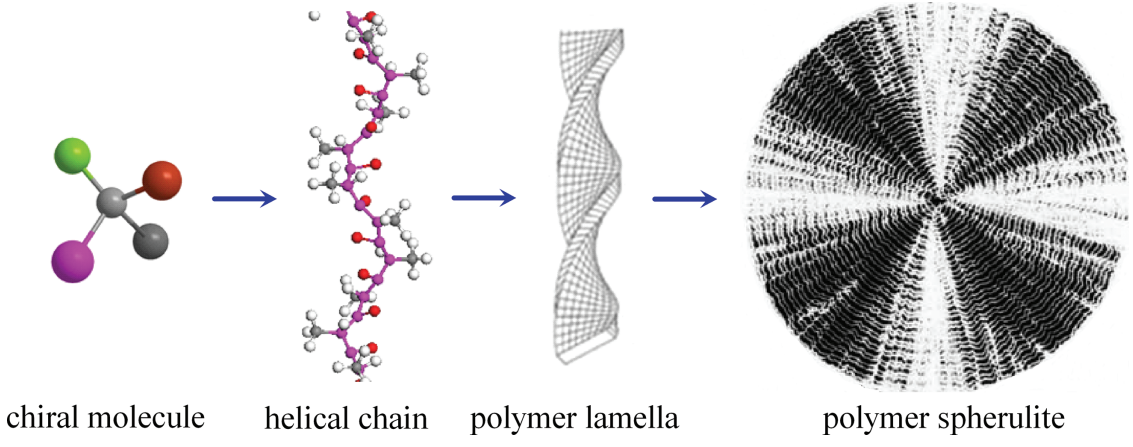

Fig. 1. Chirality translation from molecular level to morphological level. The figure of polymer spherulite is adopted with permission from [12], B. Lotz and S. Z. D. Cheng, *Polymer* 46, 577 (**2005**). © 2005, Elsevier.

ratio. For instance, the twisting strength of polymer lamellae often decreases with the thickness.[14] Moreover, if surface stresses are anisotropic, it can be expected that both the lower-level chirality and anisotropic surface stresses contribute to the formation of morphologies, but how these two factors interact is yet unclear.

Although significance of the correlation between macroscopic morphologies and the lower-level chirality has been widely recognized, very limited effort has been directed toward theoretical investigation of underlying physical mechanisms. Ou-Yang and Liu[27] derived a shape equation for helical structures of titled chiral lipid bilayers which is in analogy with cholesteric liquid crystals. Oda et al.[28] tuned the bilayer twist using chiral counterions. Using Monte Carlo simulations, Selinger et al.[24] investigated the effect of interplay between elastic forces, and the orientation and chirality of constituent molecules on shape selection in chiral self-assembly. While for chiral polymers, previous experimental findings are mainly qualitative. Moreover, controversial experimental results (e.g., chirality inversion of lamellar twisting) have been continuously reported and are still unable to be explained.[12] Recently, a relationship has been established between the molecular chirality of poly(lactide)s and their macroscopic lamellar twisting.[19] Unfortunately, the quantitative interaction between the morphological chirality and lower-level chirality is still an open issue.

In this paper, a continuum mechanics model is developed to investigate the chirality transfer from the constituent elements to the geometric morphology of quasi-one-dimensional materials. It is based on the theory of noncentrosymmetric micropolar elasticity theory. The interaction between lower-level chirality and anisotropic surface stresses is discussed to account for the handedness inversion and size effect of twisting polymer lamellas. Some controversial experimental results on the correlation between chirality at lower and higher structural levels is clearly explained by means of the proposed model. In addition, our study shows that it is possible to design and tune the micro-/nanosized chiral morphologies through chirality transfer and surface treatments.

2. CONTINUUM MODEL OF CHIRALITY TRANSFER

2.1. Surface Elastic Model for Nanoscale Chiral Materials

As aforementioned, the chirality transfer in materials usually involves complicated interactions at different length scales, and many factors influence the morphological formation at the macro scale. Atomistic studies such as molecular dynamic simulations can provide some important results in the transfer from chiral molecules to asymmetric morphology of materials. However, atomistic studies are generally very time-consuming, especially for materials with large size and complex structures. To gain a fundamental and quantitative understanding of chirality transfer, therefore, we here present a phenomenological model to rationalize the dominant physical mechanisms. For simplicity, the repeat units at the lower structural level (e.g., chiral molecular aggregates, helical chains, and twisted microfibres) will be viewed as identical chiral elements.

Consider a chiral nanowire of wideth b, thickness h, and length l ($l \gg b \gg h$), as shown in Figure 2. It is made of chiral elements assembled in an ordered or random manner. During the synthesis or growth process of the material, a certain amount of growth stresses may occur due to such reasons as temperature change, inhomogeneous concentration distributions, and residual surface stress. Under the action of the growth stresses, chiral elements will deform in a more complex manner than those without chirality. For example, they can exhibit both elongation and torsion under axial tension, rendering a chiral morphology. Here, the nanowire is modeled as a beam with rectangular cross-section. For simplicity, a uniaxial force F is applied at its two ends to model the growth stress, though more complicated loads can be analyzed similarly. The bulk material of the nanobeam is viewed as a self-assembly or aggregate of a sufficient large number of chiral microelements. Because of the internal degrees of freedom such as microrotation and elongation, chiral elements can transmit both the forces and moments. Therefore the bulk materials of the nanobeam can be treated as a hemitropic micropolar continuum.[29, 30] The same is true for the elements at its surface layer (i.e., the amorphous layer of polymer). In natural analogy to the chirality of the bulk material, the concept of surface chirality will be introduced to characterize the deformation behavior of the surface elements. The surface (or interface) chirality of a material can also be regarded as an effective property contributed from all its chiral surface (or interface) elements.

For such a material consisting of chiral elements, the classic elastic theory based on centrosymmetric stress–strain relation does not work well. Therefore, we here develop a noncentrosymmetric micropolar elastic model

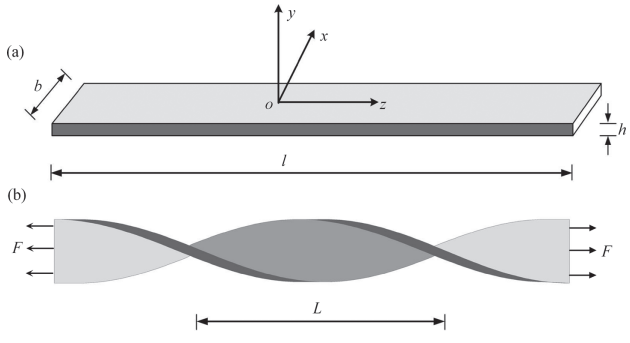

Fig. 2. A chiral nanolamella under uniaxial tension: (a) before deformation and (b) after deformation.

to describe the deformation features of chiral elements at micro and nano scales. For a nanoscale hemitropic continuum, the energy density U_{b} of bulk materials can be expressed as[29,31]

$$U_{\mathrm{b}} = \frac{1}{2}A_{ijkl}\varepsilon_{ij}\varepsilon_{kl} + \frac{1}{2}B_{ijkl}p_{ij}p_{kl} + C_{ijkl}\varepsilon_{ij}p_{kl} \tag{1}$$

where ε_{ij} is the strain tensor, p_{ij} is the curvature tensor, A_{ijkl}, B_{ijkl} and C_{ijkl} are elastic constants. Throughout this paper, Einstein's summation convention is adopted for all repeated Latin indices (1, 2, 3) and Greek indices (1, 2).

Then, the constitutive relationship can be obtained as[30–32]

$$\begin{aligned} \sigma_{ij} &= \tfrac{\partial U_{\mathrm{b}}}{\partial \varepsilon_{ij}} = A_{ijkl}\varepsilon_{kl} + C_{ijkl}p_{kl} \\ m_{ij} &= \tfrac{\partial U_{\mathrm{b}}}{\partial p_{ij}} = C_{klij}\varepsilon_{kl} + B_{ijkl}p_{kl} \end{aligned} \tag{2}$$

where σ_{ij} is the stress tensor and m_{ij} is the moment stress tensor.

To account for surface effects, Gurtin and Murdoch[32,33] established a surface elasticity theory. They treated a surface as an elastic but negligibly thin membrane, which adheres to the bulk material without slipping being allowed and has different elastic constants from the bulk. The surface stress tensor is a function of the surface strain tensor, which, in turn, depends on the deformation of the underlying bulk material. This theory has been widely adopted to elucidate the mechanical behavior of nanoscale materials.[34–40] The surface energy density U_{s} is expressed in the following form

$$\begin{aligned} U_{\mathrm{s}} &= U_{\mathrm{s}0} + \frac{\partial U_{\mathrm{s}}}{\partial \varepsilon^{\mathrm{s}}_{\alpha\beta}}\varepsilon^{\mathrm{s}}_{\alpha\beta} + \frac{\partial U_{\mathrm{s}}}{\partial p^{\mathrm{s}}_{\alpha\beta}}p^{\mathrm{s}}_{\alpha\beta} + \frac{1}{2}\frac{\partial^2 U_{\mathrm{s}}}{\partial \varepsilon^{\mathrm{s}}_{\alpha\beta}\partial \varepsilon^{\mathrm{s}}_{\gamma\delta}}\varepsilon^{\mathrm{s}}_{\alpha\beta}\varepsilon^{\mathrm{s}}_{\gamma\delta} \\ &\quad + \frac{1}{2}\frac{\partial^2 U_{\mathrm{s}}}{\partial p^{\mathrm{s}}_{\alpha\beta}\partial p^{\mathrm{s}}_{\gamma\delta}}p^{\mathrm{s}}_{\alpha\beta}p^{\mathrm{s}}_{\gamma\delta} + \frac{\partial^2 U_{\mathrm{s}}}{\partial \varepsilon^{\mathrm{s}}_{\alpha\beta}\partial p^{\mathrm{s}}_{\gamma\delta}}\varepsilon^{\mathrm{s}}_{\alpha\beta}p^{\mathrm{s}}_{\gamma\delta} + \cdots \\ &= U_{\mathrm{s}0} + \Gamma^{\mathrm{s}}_{\alpha\beta}\varepsilon^{\mathrm{s}}_{\alpha\beta} + \frac{1}{2}\Gamma^{\mathrm{s}}_{\alpha\beta\gamma\delta}\varepsilon^{\mathrm{s}}_{\alpha\beta}\varepsilon^{\mathrm{s}}_{\gamma\delta} + \mathrm{T}^{\mathrm{s}}_{\alpha\beta}p^{\mathrm{s}}_{\alpha\beta} \\ &\quad + \frac{1}{2}\mathrm{T}^{\mathrm{s}}_{\alpha\beta\gamma\delta}p^{\mathrm{s}}_{\alpha\beta}p^{\mathrm{s}}_{\gamma\delta} + \Lambda^{\mathrm{s}}_{\alpha\beta\gamma\delta}\varepsilon^{\mathrm{s}}_{\alpha\beta}p^{\mathrm{s}}_{\gamma\delta} + \cdots \end{aligned} \tag{3}$$

where $\varepsilon^{\mathrm{s}}_{ij}$ and p^{s}_{ij} are surface strain tensor and surface curvature tensor, respectively. $\Gamma^{\mathrm{s}}_{\alpha\beta}$, $\mathrm{T}^{\mathrm{s}}_{\alpha\beta}$, $\Gamma^{\mathrm{s}}_{\alpha\beta\gamma\delta}$,$\Lambda^{\mathrm{s}}_{\alpha\beta\gamma\delta}$ and $\mathrm{T}^{\mathrm{s}}_{\alpha\beta\gamma\delta}$ are materials constants of surface. Then, the surface constitutive relationship reads

$$\begin{aligned} \sigma^{\mathrm{s}}_{\alpha\beta} &= \frac{\partial U_{\mathrm{s}}}{\partial \varepsilon^{\mathrm{s}}_{\alpha\beta}} = \Gamma^{\mathrm{s}}_{\alpha\beta} + \Gamma^{\mathrm{s}}_{\alpha\beta\gamma\delta}\varepsilon^{\mathrm{s}}_{\gamma\delta} + \Lambda^{\mathrm{s}}_{\alpha\beta\gamma\delta}p^{\mathrm{s}}_{\gamma\delta} \\ m^{\mathrm{s}}_{\alpha\beta} &= \frac{\partial U_{\mathrm{s}}}{\partial p^{\mathrm{s}}_{\alpha\beta}} = \mathrm{T}^{\mathrm{s}}_{\alpha\beta} + \Lambda^{\mathrm{s}}_{\gamma\delta\alpha\beta}\varepsilon^{\mathrm{s}}_{\gamma\delta} + \mathrm{T}^{\mathrm{s}}_{\alpha\beta\gamma\delta}p^{\mathrm{s}}_{\gamma\delta} \end{aligned} \tag{4}$$

where σ^{s}_{ij} and m^{s}_{ij} are the surface stress tensor and the surface moments, respectively.

Thus for a nanoscale hemitropic continuum with volume V and surface S, the total energy density H is written as

$$\begin{aligned} H &= \int_V U_{\mathrm{b}}\,dV + \int_{\mathrm{S}} U_{\mathrm{s}}\,dS \\ &= \int_V \frac{1}{2}(\sigma:\varepsilon + \mathbf{m}:\mathbf{p})\,dV \\ &\quad + \int_{\mathrm{S}}\left[U_{\mathrm{s}0} + \frac{1}{2}(\Gamma:\boldsymbol{\varepsilon}_{\mathrm{s}} + \mathbf{T}:\mathbf{p}_{\mathrm{s}} + \sigma_{\mathrm{s}}:\boldsymbol{\varepsilon}_{\mathrm{s}} + \mathbf{m}_{\mathrm{s}}:p_{\mathrm{s}})\right]dS \end{aligned} \tag{5}$$

The geometry relations and equilibrium of the bulk materials are[33]

$$\begin{aligned} &\varepsilon_{ji} = u_{i,j} - \in_{kji}\varphi_k, \quad p_{ji} = \varphi_{i,j} \\ &\sigma_{ji,i} = 0, \quad \in_{ijk}\sigma_{jk} + m_{ji,j} = 0 \end{aligned} \tag{6}$$

where u_i denotes the displacement vector, φ_i the microrotation vector, and $\in_{ijk}$ the permutation tensor.

The surface geometry relations are[39]

$$\varepsilon^{\mathrm{s}}_{\alpha\beta} = u^{\mathrm{s}}_{\alpha,\beta} - u^n\kappa_{\alpha\beta} - \varphi^n e_{\alpha\beta}, \quad p^{\mathrm{s}}_{\alpha\beta} = \varphi^{\mathrm{s}}_{\alpha,\beta} - \varphi^n\kappa_{\alpha\beta} \tag{7}$$

where u^{s}_{α} and $\varphi^{\mathrm{s}}_{\alpha}$ are the surface displacement and surface rotation vectors.

Using the principle of virtual work, one can derive the generalized Young-Laplace equation:

$$\begin{aligned} &\sigma_{\beta\alpha}n_\beta + \sigma^{\mathrm{s}}_{\beta\alpha,\beta} = 0, \quad \sigma_{ij}n_in_j = \sigma^{\mathrm{s}}_{\alpha\beta}\kappa_{\alpha\beta} \\ &m_{\beta\alpha}n_\beta + m^{\mathrm{s}}_{\beta\alpha,\beta} = 0, \quad m_{ij}n_in_j = m^{\mathrm{s}}_{\alpha\beta}\kappa_{\alpha\beta} + \sigma^{\mathrm{s}}_{\alpha\beta}e_{\alpha\beta} \end{aligned} \tag{8}$$

where n_i is the outward normal vector of the surface, and $\kappa_{\alpha\beta}$ the curvature of the surface, and $e_{\alpha\beta}$ is the surface permutation tensor. Equation (8) is consistent with that of centrosymmetric micropolar materials with surface effect.[39]

A fourth-order isotropic tensor can be decomposed as

$$D_{ijkl} = D_1\delta_{ij}\delta_{kl} + D_2\delta_{ik}\delta_{jl} + D_3\delta_{il}\delta_{jk} \tag{9}$$

Thus Eq. (2) becomes[30]

$$\begin{aligned} \sigma_{ij} &= \lambda\varepsilon_{rr}\delta_{ij} + (\mu+\eta)\varepsilon_{ij} + (\mu-\eta)\varepsilon_{ji} \\ &\quad + \xi p_{rr}\delta_{ij} + (\chi+\nu)p_{ij} + (\chi-\nu)p_{ji} \\ m_{ij} &= \xi\varepsilon_{rr}\delta_{ij} + (\chi+\nu)\varepsilon_{ij} + (\chi-\nu)\varepsilon_{ji} \\ &\quad + \upsilon p_{rr}\delta_{ij} + (\rho+\varsigma)p_{ij} + (\rho-\varsigma)p_{ji} \end{aligned} \tag{10}$$

where λ and μ are the classical Lamé constant, and η, υ, ρ and ς are the elastic constants introduced in the micropolar theory. ξ, χ and ν are material constants associated with the chirality in the bulk.

For an isotropic surface, the constitutive relationship in Eq. (4) can be similarly rewritten as

$$\begin{aligned} \sigma^{\mathrm{s}}_{\alpha\beta} &= \Gamma^{\mathrm{s}}_{\alpha\beta} + \lambda^{\mathrm{s}}\varepsilon^{\mathrm{s}}_{\gamma\gamma}\delta_{\alpha\beta} + (\mu^{\mathrm{s}}+\eta^{\mathrm{s}})\varepsilon^{\mathrm{s}}_{\alpha\beta} + (\mu^{\mathrm{s}}-\eta^{\mathrm{s}})\varepsilon^{\mathrm{s}}_{\beta\alpha} \\ &\quad + \xi^{\mathrm{s}}p^{\mathrm{s}}_{\gamma\gamma}\delta_{\alpha\beta} + (\chi^{\mathrm{s}}+\nu^{\mathrm{s}})p^{\mathrm{s}}_{\alpha\beta} + (\chi^{\mathrm{s}}-\nu^{\mathrm{s}})p^{\mathrm{s}}_{\beta\alpha} \\ m^{\mathrm{s}}_{\alpha\beta} &= \mathrm{T}^{\mathrm{s}}_{\alpha\beta} + \xi^{\mathrm{s}}\varepsilon^{\mathrm{s}}_{\gamma\gamma}\delta_{\alpha\beta} + (\chi^{\mathrm{s}}+\nu^{\mathrm{s}})\varepsilon^{\mathrm{s}}_{\alpha\beta} + (\chi^{\mathrm{s}}-\nu^{\mathrm{s}})\varepsilon^{\mathrm{s}}_{\beta\alpha} \\ &\quad + \upsilon^{\mathrm{s}}p^{\mathrm{s}}_{\gamma\gamma}\delta_{ij} + (\rho^{\mathrm{s}}+\varsigma^{\mathrm{s}})p^{\mathrm{s}}_{\alpha\beta} + (\rho^{\mathrm{s}}-\varsigma^{\mathrm{s}})p^{\mathrm{s}}_{\beta\alpha} \end{aligned} \tag{11}$$

where λ^{s}, μ^{s}, η^{s}, υ^{s}, ρ^{s} and ς^{s} are surface elastic constants. ξ^{s}, χ^{s} and ν^{s} are material constants associated with the chirality in the surface layer.

2.2. Isotropic Surface Stress Case

For a chiral nanowire with $l \gg b \gg h$, it is reasonable to assume that among the displacement and microrotation components, only those along the z direction, u_z and φ_z, are nonzero. The stress component σ_z and the couple stress component m_z can be expressed by the axial strain ε and the twist angle per unit length τ as

$$\begin{aligned} \sigma_z &= (\lambda+2\mu)\varepsilon+(\xi+2\chi)\tau \\ m_z &= (\xi+2\chi)\varepsilon+(\upsilon+2\rho)\tau \end{aligned} \tag{12}$$

From Eq. (11), the surface stress and surface couple stress are

$$\begin{aligned} \sigma_z^{\mathrm{s}} &= (\lambda_{\mathrm{s}}+2\mu_{\mathrm{s}})\varepsilon+(\xi_{\mathrm{s}}+2\chi_{\mathrm{s}})\tau \\ m_z^{\mathrm{s}} &= (\xi_{\mathrm{s}}+2\chi_{\mathrm{s}})\varepsilon+(\upsilon_{\mathrm{s}}+2\rho_{\mathrm{s}})\tau \end{aligned} \tag{13}$$

For the tension-twist coupled deformation of quasi-one-dimensional nanomaterials, Eqs. (6) and (8) are satisfied automatically.

The potential energy of the nanobeam includes the potential energy of the applied force, the elastic strain energies in the surface layers and in the bulk. Then it is expressed as

$$\begin{aligned} H = &\frac{1}{2}(M_1\varepsilon^2+M_2\tau\varepsilon)bhl+\frac{1}{2}(M_3\tau^2+M_2\tau\varepsilon)bhl \\ &+(M_1^{\mathrm{s}}\varepsilon^2+M_2^{\mathrm{s}}\tau\varepsilon)bl+(M_3^{\mathrm{s}}\tau^2+M_2^{\mathrm{s}}\tau\varepsilon)bl-F\varepsilon l \end{aligned} \tag{14}$$

where

$$\begin{aligned} M_1 &= \lambda+2\mu, \quad M_2 = \xi+2\chi, \quad M_3 = \upsilon+2\rho \\ M_1^{\mathrm{s}} &= \lambda_{\mathrm{s}}+2\mu_{\mathrm{s}}, \quad M_2^{\mathrm{s}} = \xi_{\mathrm{s}}+2\chi_{\mathrm{s}}, \quad M_3^{\mathrm{s}} = \upsilon_{\mathrm{s}}+2\rho_{\mathrm{s}} \end{aligned} \tag{15}$$

and M_2^{s} phenomenologically considers the effect of materials chirality of surface.

At the equilibrium state, the potential energy in Eq. (14) can reach its minimal value. Making the variation with respect to ε and τ to be zero gives

$$\begin{aligned} (M_1h+2M_1^{\mathrm{s}})\varepsilon+(M_2h+2M_2^{\mathrm{s}})\tau &= \sigma_0 h, \\ (M_2h+2M_2^{\mathrm{s}})\varepsilon+(M_3h+2M_3^{\mathrm{s}})\tau &= 0 \end{aligned} \tag{16}$$

where $\sigma_0 = F/(bh)$.

The second equation of (16) can be rewritten as

$$\tau = Q\varepsilon \tag{17}$$

where the tension-twisting coupling constant Q due to material chirality is

$$Q = -\frac{M_2h+2M_2^{\mathrm{s}}}{M_3h+2M_3^{\mathrm{s}}} \tag{18}$$

From Eq. (16), we can determine the strain ε and the twist angle per unit length τ as

$$\begin{aligned} \varepsilon &= -\frac{M_3h^2+2M_3^{\mathrm{s}}h}{(M_2h+2M_2^{\mathrm{s}})^2-(M_1h+2M_1^{\mathrm{s}})(M_3h+2M_3^{\mathrm{s}})}\sigma_0 \\ \tau &= \frac{M_2h^2+2M_2^{\mathrm{s}}h}{(M_2h+2M_2^{\mathrm{s}})^2-(M_1h+2M_1^{\mathrm{s}})(M_3h+2M_3^{\mathrm{s}})}\sigma_0 \end{aligned} \tag{19a-b}$$

Since $\tau = \pi/L$, the half twist pitch length L can be given as

$$L = \frac{\pi}{\sigma_0}\frac{(M_2h+2M_2^{\mathrm{s}})^2-(M_1h+2M_1^{\mathrm{s}})(M_3h+2M_3^{\mathrm{s}})}{M_2h^2+2M_2^{\mathrm{s}}h} \tag{20}$$

Similarly, for a chiral nanofibre with circular cross section with radius r, the half twist pitch length L is

$$L = \frac{\pi}{\sigma_0}\frac{(M_2r+2M_2^{\mathrm{s}})^2-(M_1r+2M_1^{\mathrm{s}})(M_3r+2M_3^{\mathrm{s}})}{M_2r^2+2M_2^{\mathrm{s}}r} \tag{21}$$

It is emphasized that the nanobeam can also twist when subjected to a compression force. The corresponding expression of L is the same as Eq. (20) except that σ_0 should be replaced by $-\sigma_0$.

To examine the effect of lower-level chirality on the twisting morphology, we utilize the bulk chirality parameter C_{h} defined by Sharma[30] to characterize the degree of chirality in the bulk material. It is expressed as

$$C_{\mathrm{h}} = \frac{M_2^2}{M_1M_3} \tag{22}$$

where $0 \le C_{\mathrm{h}} \le 1.0$. $C = 0$ indicates the absence of chirality, and $C_{\mathrm{h}} = 1.0$ corresponds to a material with the highest degree of chirality. From Eqs. (20) and (22), the half twist pitch length L_{bulk} without surface effect is obtained as

$$L_{\mathrm{bulk}} = \frac{\pi}{\sigma_0}\frac{C_{\mathrm{h}}-1}{\sqrt{C_{\mathrm{h}}}}\sqrt{M_1M_3} \tag{23}$$

Similarly, we define the surface chirality parameter $C_{\mathrm{h}}^{\mathrm{s}}$ to stand for the degree of the effective chirality of a surface:

$$(C_{\mathrm{h}}^{s})^2 = \frac{(M_2^{\mathrm{s}})^2}{|M_1^{\mathrm{s}}M_3^{\mathrm{s}}|} \tag{24}$$

The value of $C_{\mathrm{h}}^{\mathrm{s}}$ can be either negative or positive, and is not necessarily limited in the range from 0 to 1. From Eq. (24), M_2^{s} can expressed as

$$M_2^{\mathrm{s}} = C_{\mathrm{h}}^{\mathrm{s}}\sqrt{|M_1^{\mathrm{s}}M_3^{\mathrm{s}}|} \tag{25}$$

As aforementioned, both the lower-level chirality and surface effect have been introduced phenomenologically into the elastic constants M_2 and M_2^{s}. It is seen from Eq. (20) that when M_2 and M_2^{s} vanish, L will become infinite and the nanobeam will keep straight. This means that the morphology chirality of twisted nanobeam is derived from other chirality at lower-level structures (e.g., chiral molecules aggregates and helical chains). Moreover, the

pitch length and handedness of the chiral morphology depends not only on the chirality of the material itself but also on surface effects. For this reason, both right- and left-handed chiral morphologies can be achieved for nanowires composed of molecules with identical chirality, as has been demonstrated by our recent experiments.[15]

2.3. Anisotropic Surface Stress Case

For many materials such as chiral polymer, surface stresses are usually anisotropic due to such reasons as oriental folding of molecular chains and crystallographic directions. Here, we only consider the anisotropy of surface stresses in this paper. In this case, Eq. (4) becomes

$$\begin{aligned}\sigma^{\mathrm{s}}_{\alpha\beta} &= \Gamma^{\mathrm{s}}_{\alpha\beta}+\Gamma^{\mathrm{s}}_{\alpha\beta\gamma\delta}\varepsilon^{\mathrm{s}}_{\alpha\beta}+\xi^{\mathrm{s}}p^{\mathrm{s}}_{\gamma\gamma}\delta_{\alpha\beta}\\ &\quad+(\chi^{\mathrm{s}}+\nu^{\mathrm{s}})p^{\mathrm{s}}_{\alpha\beta}+(\chi^{\mathrm{s}}-\nu^{\mathrm{s}})p^{\mathrm{s}}_{\beta\alpha}\\ m^{\mathrm{s}}_{\alpha\beta} &= \mathrm{T}^{\mathrm{s}}_{\alpha\beta}+\xi^{\mathrm{s}}\varepsilon_{\gamma\gamma}\delta_{\alpha\beta}+(\chi^{\mathrm{s}}+\nu^{\mathrm{s}})\varepsilon^{\mathrm{s}}_{\alpha\beta}+(\chi^{\mathrm{s}}-\nu^{\mathrm{s}})\varepsilon^{\mathrm{s}}_{\beta\alpha}\\ &\quad+\upsilon^{\mathrm{s}}p^{\mathrm{s}}_{\gamma\gamma}\delta_{ij}+(\rho^{\mathrm{s}}+\varsigma^{\mathrm{s}})p^{\mathrm{s}}_{\alpha\beta}+(\rho^{\mathrm{s}}-\varsigma^{\mathrm{s}})p^{\mathrm{s}}_{\beta\alpha}\end{aligned} \tag{26}$$

As shown in Figure 3, the front and the back surfaces of the nanowire are denoted by s^+ and s^-, respectively. The two surfaces may have different elastic properties due to the growth processes and chain folding manners. For simplicity, assume the two surfaces have different anisotropic elastic properties and their main elastic axes have different orientations. Refer to the global Cartesian coordinate system $(o-xyz)$ in Figure 3, where the x and z axes are along the width and length directions, respectively. The main axes of the constitutive relation on the initial front surface s^+ are along the x^+ and z^+ axes, with an angle θ^+ measured from z to z^+, whereas the main axes on the back surface s^- are along the y^- and z^- axes, with an angle θ^- measured from z to z^-. Through out this paper, the superscripts "+" and "−" stand for parameters on the initial front and back surfaces, respectively.

To consider the effect of anisotropic surface stresses on the chirality transfer, we divide the twist per unit length τ of the chiral nanobeam into two parts, i.e., $\tau=\tau_1+\tau_2$, where τ_1 is the term induced by anisotropic surface stresses and τ_2 is induced by material chirality.

For a nanobeam, Eq. (26) can be further simplified as

$$\begin{aligned}&\sigma^+_{zz}=\Gamma^+_{zz}+c^+_{22}\varepsilon+c^+_{23}\tau_1 h/2+(\xi^{\mathrm{s}}+2\chi^{\mathrm{s}})\tau_2,\quad \tau^+_{xz}=c^+_{33}\tau_1 h/2\\ &\sigma^-_{zz}=\Gamma^-_{zz}+c^-_{22}\varepsilon-c^+_{23}\tau_1 h/2+(\xi^{\mathrm{s}}+2\chi^{\mathrm{s}})\tau_2,\quad \tau^-_{xz}=c^-_{33}\tau_1 h/2\\ &m^{\pm}_{zz}=(\xi^{\mathrm{s}}+2\chi^{\mathrm{s}})\varepsilon+(\upsilon^{\mathrm{s}}+2\rho^{\mathrm{s}})\tau_2,\quad \tau_2=p_{33}\end{aligned} \tag{27}$$

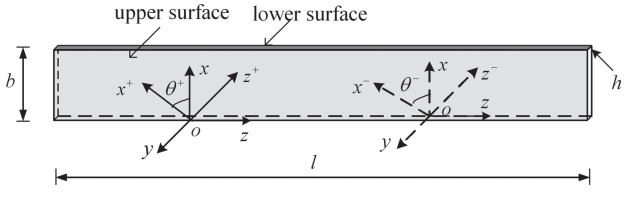

Fig. 3. A chiral nanolamella with anisotropic surface stresses on the upper and lower surfaces.

where $c^{\pm}_{ij}$ denotes the surface elastic coefficients on the two surfaces, which can be obtained through coordinate transformation. For example, c^+_{ij} can be expressed as

$$\begin{aligned}c^+_{11} &= c^{\mathrm{s}+}_{1111}\cos^4\theta^+ + 2(c^{\mathrm{s}+}_{1122}+2c^{\mathrm{s}+}_{1212})\cos^2\theta^+\sin^2\theta^+\\ &\quad+c^{\mathrm{s}+}_{2222}\sin^4\theta^+\\ c^+_{12} &= (c^{\mathrm{s}+}_{1111}+c^{\mathrm{s}+}_{2222}-4c^{\mathrm{s}+}_{1212})\cos^2\theta^+\sin^2\theta^+\\ &\quad+c^{\mathrm{s}+}_{1212}(\cos^4\theta^+ + \sin^4\theta^+)\\ c^+_{22} &= c^{\mathrm{s}+}_{1111}\sin^4\theta^+ + 2(c^{\mathrm{s}+}_{1122}+2c^{\mathrm{s}+}_{1212})\cos^2\theta^+\sin^2\theta^+\\ &\quad+c^{\mathrm{s}+}_{2222}\cos^4\theta^+\\ c^+_{31} &= (-c^{\mathrm{s}+}_{1111}+c^{\mathrm{s}+}_{1122}+2c^{\mathrm{s}+}_{1212})\cos^3\theta^+\sin\theta^+\\ &\quad+(-c^{\mathrm{s}+}_{1122}+c^{\mathrm{s}+}_{2222}-2c^{\mathrm{s}+}_{1212})\cos\theta^+\sin^3\theta^+\\ c^+_{32} &= (-c^{\mathrm{s}+}_{1111}+c^{\mathrm{s}+}_{1122}+2c^{\mathrm{s}+}_{1212})\cos\theta^+\sin^3\theta^+\\ &\quad+(-c^{\mathrm{s}+}_{1122}+c^{\mathrm{s}+}_{2222}-2c^{\mathrm{s}+}_{1212})\cos^3\theta^+\sin\theta^+\\ c^+_{33} &= \frac{1}{2}(c^{\mathrm{s}+}_{1111}+c^{\mathrm{s}+}_{2222}-2c^{\mathrm{s}+}_{1122})\sin^2 2\theta^+\\ &\quad+2c^{\mathrm{s}+}_{1212}\cos^2 2\theta^+\\ c^+_{13} &= 2c^+_{31},\quad c^+_{23}=2c^+_{32}\end{aligned} \tag{28}$$

Thus the potential energy of a chiral nanobeam with anisotropic surface stresses can be expressed as

$$\begin{aligned}H &= \frac{1}{2}[(M_1\varepsilon+M_2\tau_2)\varepsilon+(M_2\varepsilon+M_3\tau_2)\tau_2]bhl+\frac{1}{6}\mu\tau_1^2h^3bl\\ &\quad+\frac{1}{4}[2(\Gamma^+ +\Gamma^-)+2(c^+_{22}+c^-_{22})\varepsilon+(c^+_{23}-c^-_{23})\tau_1 h\\ &\quad+4M^{\mathrm{s}}_2\tau_2]\varepsilon bl+\frac{1}{8}[2(c^+_{32}-c^-_{32})\varepsilon+(c^+_{33}\\ &\quad+c^-_{33})\tau_1 h]\tau_1 bhl+(M^{\mathrm{s}}_2\varepsilon+M^{\mathrm{s}}_3\tau_2)\tau_2 bl-F\varepsilon l\end{aligned} \tag{29}$$

It should be mentioned that anisotropic surface stresses may also bend the nanobeam. For simplicity, we only consider the twisting deformation. Because for the problem of current interest, twisting deformation is dominant in a wide range of combinations of θ^+ and θ^-.

The equilibrium state can be determined by minimizing H in Eq. (29) with respect to ε, τ_1 and τ_2. The minimization of H yields

$$A\varepsilon+2B\tau_1+8C\tau_2=\sigma_0',\quad 3B\varepsilon+D\tau_1=0,\quad C\varepsilon+Q\tau_2=0 \tag{30}$$

where

$$\begin{aligned}&A=8[M_1+\frac{1}{h}(c^+_{22}+c^-_{22})],\quad B=3(c^+_{32}-c^-_{32})\\ &C=M_2+\frac{2}{h}M^{\mathrm{s}}_2,\quad D=4\mu h^2+3(c^+_{33}+c^-_{33})h\\ &Q=M_3+\frac{2}{h}M^{\mathrm{s}}_3,\quad \sigma_0'=\frac{8F}{bh}-\frac{4}{h}(\Gamma^+ +\Gamma^-)\end{aligned} \tag{31}$$

Then from Eq. (30), one can determine ε, τ_1, and τ_2 as

$$\varepsilon = \frac{QD}{AQD - 8C^2D - 6B^2Q}\sigma_0'$$
$$\tau_1 = \frac{3BQ}{8C^2D + 6B^2Q - AQD}\sigma_0' \quad (32)$$
$$\tau_2 = \frac{CD}{8C^2D + 6B^2Q - AQD}\sigma_0'$$

Thus the half twist pitch length L is

$$L(h) = \frac{\pi}{\tau_1 + \tau_2} = \frac{\pi}{\sigma_0'}\frac{6B^2Q + 8C^2D - AQD}{3BQ + CD} \quad (33)$$

Similar to Eq. (25), M_2^s can be expressed as

$$M_2^s = C_h^s\sqrt{|0.5(c_{22}^+ + c_{22}^-)M_3^s|} \quad (34)$$

For a chiral nanofibre with circular cross section of radius r, we have

$$\varepsilon = \frac{Q_1D_1}{A_1Q_1D_1 - C_1^2D_1 - 6B_1^2Q_1}\sigma_0'$$
$$\tau_1 = \frac{3B_1Q_1}{C_1^2D_1 + 6B_1^2Q_1 - A_1Q_1D_1}\sigma_0' \quad (35)$$
$$\tau_2 = \frac{C_1D_1}{C_1^2D_1 + 6B_1^2Q_1 - A_1Q_1D}\sigma_0'$$

with

$$A_1 = M_1 + \frac{1}{r}M_2^s + \frac{2}{r}c_{22}^s, \quad B_1 = c_{32}^s$$
$$C_1 = M_2 + \frac{1}{r}M_2^s, \quad D_1 = \mu r^2 + 2rc_{33}^s \quad (36)$$
$$Q_1 = M_3 + \frac{2}{r}M_3^s, \quad \sigma_1' = \frac{F}{\pi r^2} - \Gamma^s$$

Then the half twist pitch length L can be obtained as

$$L(r) = \frac{\pi}{\sigma_1'}\frac{6B_1^2Q_1 + C_1^2D_1 - A_1Q_1D_1}{3B_1Q_1 + C_1D_1} \quad (37)$$

and M_2^s is expressed in term of surface chirality parameter C_h^s as

$$M_2^s = C_h^s\sqrt{|c_{22}^sM_3^s|} \quad (38)$$

3. NUMERICAL RESULTS AND DISCUSSION

3.1. Isotropic Surface Stress Case

In this section, numerical examples will be provided to illustrate the formation of chiral shapes of nanowires. As can be seen from Eq. (21), only the values of elastic constants M_i and M_i^s $(i = 1-3)$ are needed to calculate the twisting handedness and the corresponding pitch length. For illustration, we consider a soft nanowire/nanoribbon with lower elastic moduli and micropolar elastic constants: $M_1 = 2.0 \times 10^9$ N/m^2, $M_3 = 1.0 \times 10^{-3}$ N, $M_1^s = -0.05$ N/m, and $M_3^s = 1.0 \times 10^{-11}$ Nm, which satisfy the thermodynamic restrictions on the elastic constants of chiral materials.[22] For several representative values of C_h, Figure 4 shows the variation of the half twist pitch length L with respect to the thickness of the chiral nanobeam. A positive value of L stands for the right-handedness of the twisting nanobeam, and *vice versa*. Figure 4 shows an interesting size dependence of nanowire morphology. For higher values of C_h (i.e., $C_h = 0.5, 0.6, 0.7$), an inversion of morphological chirality (twisting handedness) from left-handedness to right-handedness may occur, at which $\tau \to 0$. This means that there is a characteristic thickness of the nanoribbon, i.e., $h = h_c$, corresponding to the inversion point of the curve. However, since $L = 0$ is only a limiting case, the critical thickness at which the morphological chirality inversion occurs will be, in practice, in a range of $h_{c1} \le h_c \le h_{c2}$, where h_{c1} and h_{c2} can be determined from Eqs. (17) or (19a) under the small strain condition. In other words, nanobeams with $h < h_{c1}$ and $h > h_{c2}$ may have different morphological chiralities. It is also seen that with the increase in the nanobeam thickness, the half pitch length L decreases when $h < h_{c1}$ or increases when $h > h_{c2}$.

The effect of effective surface chirality on the inversion of morphological chirality is shown in Figure 5, where we take $h = 8.0$ nm and $C_h = 0.5$. The blue and red curves stand for the twisting of right $(L > 0)$ and left $(L < 0)$ handedness, respectively. When $C_h^s = 9.26$, the twisting handedness of the chiral nanobeam has been inversed. In addition, the twisting pitch length also varies with increasing C_h^s.

3.2. Anisotropic Surface Stress Case

As above mentioned, the chiralities in both the bulk and on the surface of a material depend on the lower-level

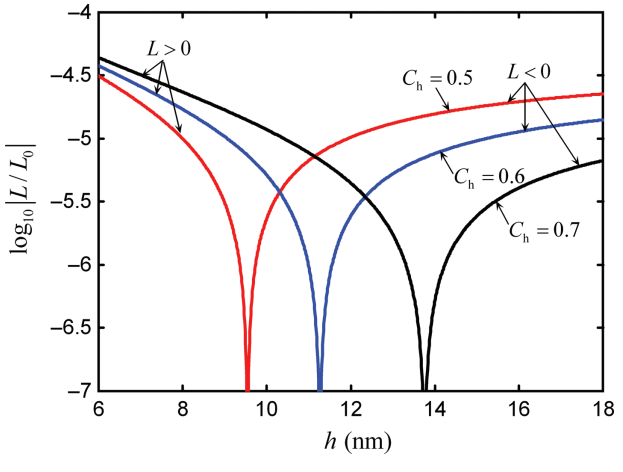

Fig. 4. Twisting pitch and the inversion of twisting handedness of a chiral nanobeam.

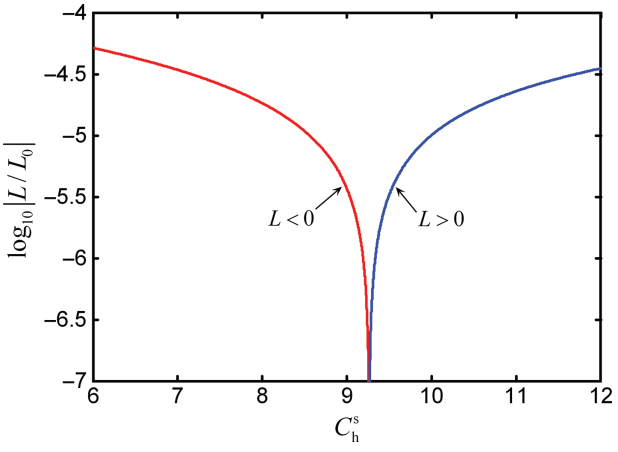

Fig. 5. Inversion of morphology chirality induced by surface chirality.

chirality. For very soft polymer, the chirality in its bulk is usually weak (i.e., $C_h \approx 0$). However, nonaffine deformation and rotation of the helical chain folding in the surface layer can induce strong effective surface chirality. In this case, the interaction between anisotropic surface stresses and surface chirality will dominate the transfer of lower-level chirality to the morphological level. For illustration, we consider a chiral nanobeam with the following elastic constants in the bulk: $\lambda = 12.857$ GPa, $\mu = 3.214$ GPa, and $C_h = 0$. The orthotropic surface elastic properties can also be expressed in the form: $\Gamma^s_{1111} = \Gamma^s_{2222} = \kappa_s + \mu_s$, $\Gamma^s_{1122} = \Gamma^s_{2211} = \kappa_s - \mu_s$, and $\Gamma^s_{1212} = \Gamma^s_{1221} = (1/2)A_0(c^s_{1111} - c^s_{1122})$, where κ_s and μ_s designate the surface elastic moduli. The parameter A_0 stands for the degree of anisotropy of surface elasticity. In what follows, the surface elastic moduli are taken as: $\kappa_s = 3.49387$ N/m, $\mu_s = -5.70195$ N/m, $M^s_3 = 1.0 \times 10^{-11}$ Nm, $C^s_h = -15.0$, $A_0 = 0.1$, $\theta^+ = -0.23\pi$, and $\theta^- = 0$.

In Figure 6(a), the variation of the logarithmic normalized twist per unit length τ, τ_1 and τ_2 with respect to the thickness are plotted. A positive value of τ (τ_1 or τ_2) stands for the twisting of right handedness, and a negative value stands for left handedness. As aforementioned, τ_1 is induced by the anisotropic surface stress, while τ_2 is induced by the surface chirality. It can seen that when $h < h_c \approx 7.3$ nm, $\tau_1 > 0$, $\tau_2 < 0$, $\tau < 0$ and $|\tau_2| < |\tau| < |\tau_1|$, demonstrating the competition between anisotropic surface stresses and surface chirality. Moreover, it is seen that anisotropic surface stresses play a significant role in formation of chiral morphologies. When $h > h_c \approx 7.3$ nm, one has $\tau_1 < 0$, $\tau_2 > 0$ and $\tau < 0$. Thus, it is concluded that the chiral morphologies of nanowires may be determined by the competition interaction between anisotropic surface stresses and surface chirality. In addition, the chirality transfer exhibits a distinct size effect.

If we change the sign of surface chirality (i.e., $C^s_h = 15.0$) and keep other material parameters unchanged, anisotropic surface stresses and surface chirality will have a cooperative interaction in the chirality transfer, as shown

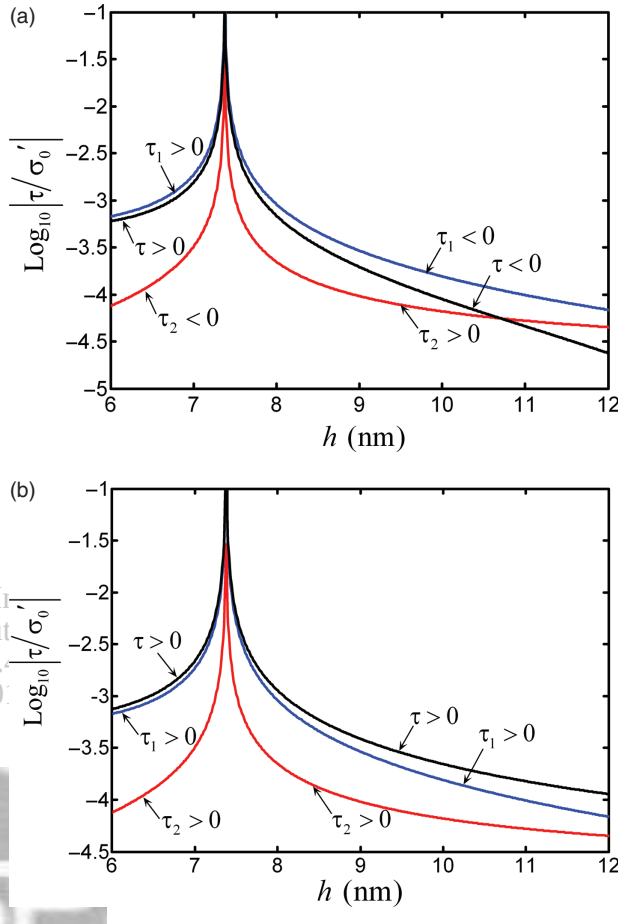

Fig. 6. (a) Lamellar twisting induced by competition between surface chirality and anisotropic surface stress. (b) Lamellar twisting induced by cooperative interaction between surface chirality and anisotropic surface stress.

in Figure 6(b). It can be seen that the values of τ, τ_1 and τ_2 have the same signs, and $|\tau| > |\tau_1| > |\tau_2|$. Similar to Figure 6(a), when $h < h_c \approx 7.3$ nm, the anisotropic surface stresses dominate the formation of chiral morphologies, and when $h > h_c \approx 7.3$ nm, surface chirality become playing a more important role.

For some nanomaterials or self-assembled systems, chiral elements can have certain structural rigidity, which may induce high bulk chirality. To consider the interaction between anisotropic surface stresses and bulk chirality, we assume that the surface chirality is very weak and neglected in this example (i.e., $C^s_h = 0$). For illustration, we take the following parameters: $C_h = 0.9$, $A_0 = 0.2$, $M^s_3 = 0$, $\theta^+ = 0.1\pi$, and the other properties are the same as above. Figure 7(a) gives the variations of the half twist pitch lengths L, L_1 and L_2 with respect to the thickness of the nanobeam. L_1 is induced from anisotropic surface stresses, and L_2 from bulk chirality. It can be found that the competition interaction between anisotropic surface stress and bulk chirality may induce opposite handedness. When $h <$ 8.0 nm, the half twist pitch length L is mainly determined by anisotropic surface stresses. When $h > 8.0$ nm, the

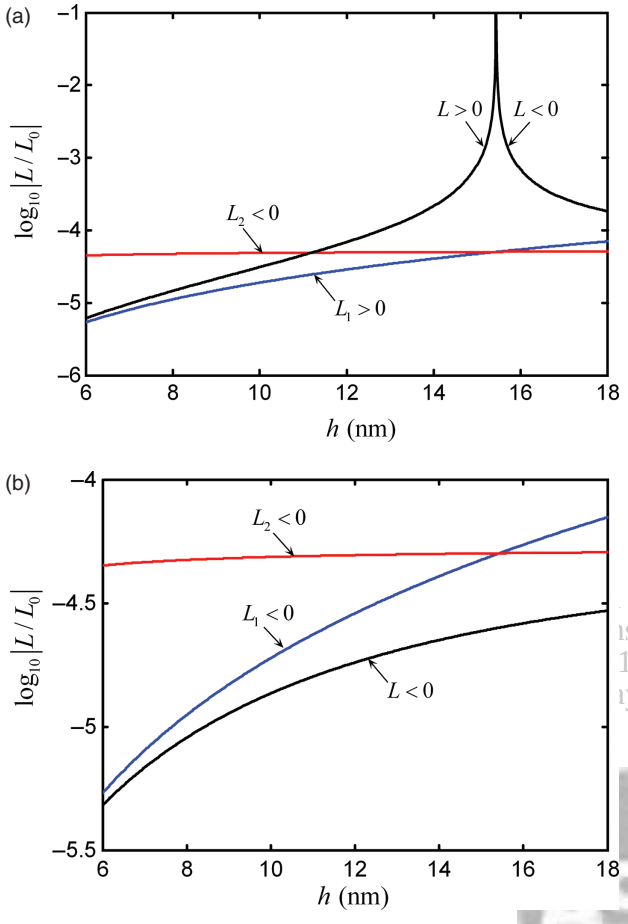

Fig. 7. (a) Lamellar twisting induced by competition between bulk chirality and anisotropic surface stress. (b) Lamellar twisting induced by cooperative interaction between bulk chirality and anisotropic surface stress.

effect of anisotropic surface stresses become weak and the bulk chirality dominates the twisting morphology of the nanobeam. At the intersection point of the blue and red lines, L_1 and L_2 have the same value but opposite handedness, and the half twist pitch length L become infinite due to their competition. In other words, the twist chirality of the nanobeam is inversed at this point.

In Figure 7(b), the variation of L, L_1 and L_2 with respect to the thickness of nanobeam are plotted under $\theta^+ = -0.1\pi$. Due to the change of the orientation of surface anisotropy, the twist chirality induced by the anisotropic surface stresses becomes left handedness ($L_1 < 0$) from right handedness as shown in Figure 6(a). Thus, the anisotropic surface and bulk chirality may also have a cooperative contribution to the chirality and size of twisted nanobeams. Similar to that in Figure 6(a), the contribution from the bulk chirality will become larger along with increasing thickness.

The above results demonstrate that both the lower-level chirality and anisotropic surface stresses contribute to the chirality transfer in quasi-one-dimensional nanomaterials with anisotropic surface elasticity. For micro- or nanosized materials with hierarchical chiral structures, chirality often sweeps through several structural levels.

4. CONCLUSIONS

We have developed a continuum mechanics model to phenomenologically investigate the chirality transfer from the lower-level structures to the morphologies of quasi-one-dimensional materials. It is found that the handedness and the corresponding characteristic size of chiral morphology depend not only on the chirality of constituent elements but also on surface effects. Both the effects of anisotropic surface stresses and surface chirality or bulk chirality have been investigated. The inversion of morphological chirality and some size dependent phenomena can be interpreted by considering the interaction of these two mechanisms. The model presented in this paper can predict the formation of chiral morphologies at micro and nano scales. It can also provide a possible explanation for the observed conflicting experimental results on the correlation between lower-level chirality and morphological chirality. To further investigate the chirality transfer on the lower levels of quasi-one-dimensional nanomaterials and self-assembled systems, the arrangement of chiral molecules and their interactions should be considered.

Acknowledgments: This work was supported by the National Natural Science Foundation of China (Grant Nos. 10802041, 107032050 and 10525210), 973 Program of MOST (2010CB631005) and Innovation Foundation of Tianjin University (Young Teacher Foundation of Tianjin University). The authors also thank Professor Ganyun Huang for helpful suggestions.

References

1. L. Pasteur, *Ann. Chim. Phys.* 24, 442 (**1848**).
2. W. J. Lough and I. W. Wainer, Chirality in Natural and Applied Science, Blackwell Science, Oxford (**2002**).
3. Y. Liu and J. Han, *Phys. Rev. Lett.* 854, 154 (**2000**).
4. E. L. Ivchenko and B. Spivak, *Phys. Rev. B* 66, 155404 (**2002**).
5. X. P. Gao, Y. Ding, W. J. Mai, W. L. Hughes, C. S. Lao, and Z. L. Wang, *Science* 309, 1700 (**2005**).
6. D. Q. Zhang, A. Alkhateeb, H. M. Han, H. Mathmood, and D. N. McIlroy, *Nano Lett.* 3, 983 (**2003**).
7. J. Zhu, H. L. Peng, A. F. Marshall, D. M. Barnett, W. D. Nix, and Y. Cui, *Nat. Nanotechnol.* 3, 477 (**2008**).
8. A. F. D. Fonseca, C. P. Malta, and D. S. Galvão, *Nanotechnology* 17, 5620 (**2006**).
9. K. Cahill, *Phys. Rev. E* 72, 062901 (**2005**).
10. Y. Snir and R. D. Kamien, *Science* 307, 1067 (**2005**).
11. D. N. McIlroy, D. Zhang, and Y. Kranov, *Appl. Phys. Lett.* 79, 1540 (**2001**).
12. B. Lotz and S. Z. D. Cheng, *Polymer* 46, 577 (**2005**).
13. J. S. Wang, X. Q. Feng, G. F. Wang, and S. W. Yu, *Appl. Phys. Lett.* 92, 151916 (**2008**).
14. H. M. Ye, J. S. Wang, J. Xu, X. Q. Feng, B. H. Guo, X. M. Xie, J. J. Zhou, L. Lin, Q. Wu, and G. Q. Chen, *Macromolecules* 43, 5762 (**2010**).

15. A. Brizard, R. Oda, and I. Huc, *Top. Curr. Chem.* 256, 167 (**2005**).
16. G. Bellesia and J. Shea, *J. Chem. Phys.* 126, 245104 (**2007**).
17. D. K. Smith, *Chem. Soc. Rev.* 38, 684 (**2009**).
18. J. V. Selinger, M. S. Spector, and J. M. Schnur, *J. Phys. Cehm. B* 105, 7157 (**2001**).
19. D. Maillard and R. E. Rrud'homme, *Macromolecules* 41, 1705 (**2008**).
20. B. Lotz, A. Gonthier-Vassal, A. Brack, J. Magoshi, *J. Mol. Biol.* 156, 345 (**1982**).
21. P. A. Maggard, C. L. Stern, and K. R. Poeppelmeier, *J. Am. Chem. Soc.* 123, 7742 (**2001**).
22. W. Helfrich, *Langmuir* 7, 567 (**1991**).
23. R. Fasel, M. Parchau, and K. Ernst, *Angew. Chem. Int. Ed.* 42, 5178 (**2003**).
24. R. L. B. Selinger, J. V. Selinger, A. P. Malanoski, and J. M. Schnur, *Phys. Rev. Lett.* 93, 158103 (**2004**).
25. H. M. Ye, J. Xu, B. H. Guo, and T. Iwata, *Macromolecules* 42, 694 (**2009**).
26. G. Gilat, *J. Phys. A: Math. Gen.* 22, L545 (**1989**).
27. Z. C. Ou-Yang and J. X. Liu, *Phys. Rev. Lett.* 65, 1679 (**1990**).
28. R. Oda, T. Huc, M. Schmutz, S. J. Candau, and F. C. MacKintosh, *Nature* 399, 566 (**1999**).
29. R. S. Lakes and R. L. Benedict, *Int. J. Eng. Sci.* 29, 1161 (**1982**).
30. P. Sharma, *Int. J. Solids Struct.* 41, 6317 (**2004**).
31. W. Nowacki, Theory of Asymmetric Elasticity, Polish-Scientific Publishers, Warszawa and Pergamon Press (**1986**).
32. M. E. Gurtin and A. I. Murdoch, *Arch. Ration. Mech. Anal.* 57, 291 (**1975**).
33. M. E. Gurtin, J. Weissmüller, and F. Larché, *Phil. Mag. A* 78, 1093 (**1995**).
34. P. Sharma, S. Ganti, and N. Bhate, *Appl. Phys. Lett.* 82, 535 (**2003**).
35. V. B. Shenoy, *Int. J. Solids Struct.* 39, 4039 (**2002**).
36. G. F. Wang, X. Q. Feng, and S. Y. Yu, *EPL* 77, 44002 (**2007**).
37. G. F. Wang and X. Q. Feng, *Appl. Phys. Lett.* 90, 231904 (**2007**).
38. L. H. He, C. W. Lim, and B. S. Wu, *Int. J. Solids Struct.* 41, 847 (**2004**).
39. H. Chen, G. K. Hu, and Z. P. Huang, *Int. J. Solids Struct.* 44, 8106 (**2007**).
40. C. Q. Ru, *Appl. Phys. Lett.* 94, 051905 (**2009**).

Received: 23 May 2010. Accepted: 24 June 2010.